# Theoretical Study on the Photochemical Behavior of 4-(Dimethylamino)benzonitrile

**Yoshiaki Amatatsu***

*Faculty of Engineering and Resource Science, Akita University, Tegata Gakuen-cho, Akita 010-8502, Japan*

*Received: March 3, 2005; In Final Form: May 6, 2005*

Ab initio calculations have been performed to examine the photochemical behavior of 4-(dimethylamino)-benzenzonitrile (DMABN). The conical intersection between $S_2$ and $S_1$ ($S_2/S_1-$CIX), where the internal conversion takes place after the main transition of $S_0-S_2$ at the equilibrium geometry in $S_0$, is characterized by a dimethylamino-twisted quinoid structure where aromaticity of the benzene ring is lost. The optimized geometry of the charge transfer (CT) state in $S_1$ has a feature similar to that of $S_2/S_1-$CIX but is not energetically stabilized so much. Consequently, electronically excited DMABN with CT character relaxes into the most stable locally excited (LE) state in $S_1$ through a recrossing at $S_2/S_1-$CIX in gas phase or nonpolar solvent. In polar solvent, in contrast, the equilibration between LE and CT takes place in $S_1$ so that the CT state is more stable because of electrostatic interaction. The excited states of DMABN derivatives have been also examined. On the basis of the present computational results, a new and simple guiding principle of the emission properties is proposed, where conventional twisted intramolecular CT (TICT) and planar intramolecular CT (PICT) models are properly incorporated.

## 1. Introduction

The formation of the photoinduced charge transfer (CT) state has been of great interest in chemistry, biology, and material science. As a typical example, the photochemistry of 4-(dimethylamino)benzonitrile (DMABN) has been extensively studied from both experiment and theory since the finding of the dual fluorescence in polar solvent by Lippert et al.[1] In nonpolar solvent, a normal fluorescence assigned to the locally excited (LE) state is observed, whereas a second fluorescence with anomaly red shift comes to be observed in polar solvent. They assigned the anomaly red-shifted fluorescence to a CT state with large dipole moment. Following their finding, many experimental and theoretical works have been done to examine the geometrical structure of the CT state.

The twisted intramolecular CT (TICT) model, which was proposed by Grabowski et al.[2] and forwarded by Rettig's group,[3−5] has been a most promising candidate for the species with anomaly red-shifted fluorescence in polar solvent. In the TICT model, the CT state is supposed to be stabilized by a geometrical twist between the dimethylamino and the remaining part ($\tau$ in Figure 1). As an alternative model, the planar intramolecular CT (PICT) model has been advocated by Zachariasse's group for the last several years.[6−12] In the PICT model, the energy gap between $S_1$ (LE) and $S_2$ (CT) in the Franck−Condon (FC) region determines the capability of CT formation. That is, a small energy gap leads to a CT formation through the vibronic interaction induced by the amino wagging motion. In this model, the torsional motion of the amino group is not supposed to be an essential factor and instead the wagging motion for a planar conformation of the amino group is important. They examined the emission properties of several rigid DMABN derivatives that are prevented from the torsional motion of the amino group. Thereby, they observed that a rigidized DMABN derivative of 1-*tert*-butyl-6-cyanotetrahydroquinoline (abbreviated by NTC6) exhibits a CT emission even in nonpolar solvent. The following two models are nowadays minor. The rehybridization intramolecular CT (RICT) model was proposed by Sobolewski and Domcke.[13−15] In RICT model, the in-plane bent structure of the acceptor group (CN in this case) changes the hybridizations of atoms from sp into $sp^2$ and consequently stabilizes the CT state. The wagged intramolecular CT (WICT) model by Gorse and Pesquer[16] is supposed for the highly wagged amino group to be electronically decoupled with the other part, leading to a CT state with large dipole moment. However, the last two models has been ruled out by some experiments and calculations.[5,7,17−19]

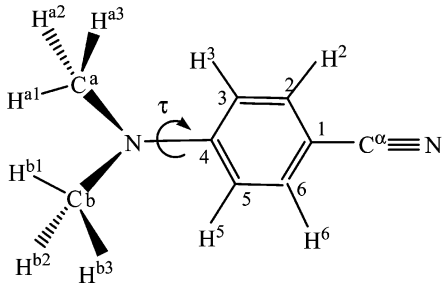


**Figure 1.** Numberings of atoms of DMABN. The torsional angle $\tau$ is defined by the dihedral angle between two planes of which normal vectors are $\{\mathbf{r}(C^4C^5) \times \mathbf{r}(C^4C^3)\} \times \mathbf{r}(C^4N)$ and $\{\mathbf{r}(NC^a) \times \mathbf{r}(NC^b)\} \times \mathbf{r}(NC^4)$.

Many spectroscopic approaches have been done to check the validity of the models mentioned above. Kajimoto and coworkers examined the possibility of a CT formation about DMABN, the related molecules, and their van der Waals clusters with solvent molecules by means of supersonic jet spectroscopic technique.[20,21] They found that electronically excited DMABN through the 0−0 transition exhibits no CT fluorescence, whereas 4-(dimethylamino)-3,5-dimethylbenzonitrile, where the dimethylamino group is pretwisted even in $S_0$, exhibits a red-shifted CT fluorescence. They also determined the geometry in $S_1$ by means of microwave and laser spectroscopic techniques.[22]

* Corresponding author. E-mail: amatatsu@ipc.akita-u.ac.jp. Fax: +81-18-889-2601. Phone: +81-18-889-2625.

10.1021/jp051083e CCC: $30.25 
Published on Web 07/27/2005

The dimethylamino group in $S_1$ is twisted by 30° against the benzene plane, and it changes from a pyramidal to a planar structure. Recently, Saigusa and co-workers revised the twisted angle into 26.2°.[23] The time-resolved spectroscopic measurements gave new insight into the temporal behavior of electronically excited DMABN. Hashimoto and Hamaguchi examined the behavior of the triplet state on a time scale of nanoseconds.[24] They found that, in the triplet TICT state as well as singlet one, the C≡N stretch is shifted down by 120 $cm^{-1}$ in polar solvent. This is attributed to a weakening of the C≡N bond caused by the electron flow from the other part. In nonpolar solvent, on the other hand, only one transient species, assigned to a non-CT triplet, is observed. On a shorter time scale of picoseconds, more delicate electronic and geometrical information on electronically excited DMABN was unraveled. Kwok et al. characterized the LE (DE in their papers) as well as CT state.[18,19,25] In the LE state, the benzene ring is enlarged and the pyramidal structure around the dimethylamino group flattens because of the enhancement of the $\pi$ conjugation between the dimethylamino and the other part. As to the CT structure, it was found that the strong ring vibration, which is similar to Wison's 8a vibration of benzene and deforms the hexagon, appears at 1585 $cm^{-1}$. The C≡N stretch is shifted from 2220 to 2096 $cm^{-1}$. By analysis of the other bands as well as the band mentioned above, they supported the TICT model. Okamoto and co-workers also obtained a similar spectrum of the CT state, which is basically of benzenoid nature with a large contribution from quinoidal structure, though they suspended a conclusion on the TICT or PICT model.[26] Despite the difference of the interpretation of the CT structure, the equilibration between CT and LE states was observed to take place on a time scale of 3−4 ps.[7,18] The recent experiment on a much shorter time scale of femtosecond gave a new insight of the photochemistry of DMABN. Fuss et al. reported that the torsional motion is very fast (68 fs) for DMABN to relax into $S_1$ at a conical intersection between $S_2$ and $S_1$ (denoted by $S_2/S_1$−CIX) after the main transition of $S_0$−$S_2$.[27] The ultrafast torsional motion to reach $S_2/S_1$−CIX radically has changed a conventional picture of the photochemistry of DMABN. That is, the equilibration process of LE ⇆ CT takes place only on the $S_1$ surface on a time scale of several picoseconds, whereas the internal conversion from the higher excited state of $S_2$ is completed during at most 100 fs without any solvent effect.

In accord with a progress of experimental techniques that allow us to obtain detailed information on the photoprocess, theoretical approaches also have been useful to deepen the understanding of the DMABN photochemistry. Most of them supported the TICT model. Kato and co-workers performed Monte Carlo and molecular dynamics simulations of electronically excited DMABN in aqueous solution by using ab initio configuration interaction potentials.[28,29] Roos' group performed large scale calculations of complete active space self-consistent field (CASSCF) and its second-order perturbation to characterize and quantify the LE and CT states.[30] Tomasi and co-workers applied their original polarized continuum model (PCM) to the DMABN photochemistry to treat the DMABN system in polar solvent realistically by means of ab initio CASSCF calculations.[31] Very recently, Rappoport and Furche applied the time-dependent density functional theory (TDDFT) to calculate the reaction path which is obtained by geometry optimizations as a function of dimethylamino torsional angle in the excited states.[32]

Despite much effort to elucidate the photochemistry of DMABN, there continues to be serious controversy between TICT and PICT models. So our present purpose is to propose a new and reasonable picture of the photochemical behavior of DMABN in gas phase, nonpolar and polar solvent by means of reliable ab initio methods. The present paper is organized as follows. In the next section, we describe the method of calculations. In section 3, we mention both electronic and geometrical structures at important conformations including $S_2/S_1$−CIX. Then we discuss and present a new model of the photochemical behavior of DMABN in gas phase, nonpolar and polar solvents. We further compare our model with conventional PICT and TICT models. Last of all, we give a summary on the present computational results.

## 2. Method of Calculations

We performed the CASSCF calculations where all six $\pi$ occupied orbitals (including one lone pair orbital on N-atom of the amino group) and the lowest five $\pi^*$ unoccupied orbitals are taken into account as the active space (i.e., twelve electrons in eleven orbitals CASSCF denoted by (12,11)CASSCF). In some cases, we made energetic corrections by second-order multireference Möller−Plesset (MRMP2) calculation to do a quantitative discussion. First, we did the geometry optimizations at several important conformations in each electronic state, such as a geometry in $S_0$ (denoted by $S_0$-geometry), $S_2/S_1$−CIX. Then we scanned the potential energy surfaces of $S_1$ and $S_2$ by means of the two-state averaged (12,11)CASSCF (denoted by SA2-(12,11)CASSCF) where the two-particle density matrixes in $S_1$ and $S_2$ are equally weighted. Furthermore, we followed the intrinsic reaction coordinate from $S_2/S_1$−CIX to examine the dynamical behavior in the relaxation process. Additionally, we did the optimizations of the first two excited states of 1B and 2A under $C_2$ symmetry.

As described in Introduction, an important topic in the DMABN photochemistry is about the geometry from which the fluorescence is anomaly red-shifted due to a CT state formation in polar solvent. To examine it, we calculated the free energies by means of (12,11)CASSCF combined with PCM method. In the present evaluation of the free energies, we took account of only the electrostatic interaction between DMABN and solvent. The others, such as dispersion and repulsion terms, were neglected. Because, in a related system of 4-(ditheylamino)-4′-cyanostilbene,[33,34] we had an experience that the evaluation of these terms is much more computationally demanding than that of the electrostatic term and nevertheless they are almost constant as a function of the torsional angle. Therefore, the free energy is evaluated by the following expression:

$$F_i = \langle \psi_i | H_0 + V/2 | \psi_i \rangle \quad (1)$$

where $\langle \psi_i | H_0 | \psi_i \rangle$ and $\langle \psi_i | V/2 | \psi_i \rangle$ are the internal energy in the solvent and electrostatic interaction in the $S_i$ state, respectively.

The basis set used in these calculations is the Huzinaga−Dunning double-$\zeta$ (DZ) basis set, where polarization on carbon ($\alpha_d = 0.75$), except for those of the methyl groups, and the nitrogen ($\alpha_d = 0.80$) atoms were added to ensure the flexibility of the $\pi$ and lone pair electrons derived from them. We used GAMESS program in the present ab initio calculations,[35] except for the location of $S_2/S_1$−CIX by Gaussian 03.[36]

## 3. Results

First of all, we mention the electronic structures of DMABN at $S_0$-geometry. In Table 1, we listed the excitation energies, dipole moments, oscillator strengths, and the main configuration

**TABLE 1: Excitation Energies, Dipole Moments and the Main CSFs of DMABN at $S_0$-Geometry[a]**

| | excitation energy (eV) | | | dipole moment | oscillator | |
|---|---|---|---|---|---|---|
| | CASSCF | MRMP2 | expl | (Debye) | strength[b] | main CSFs[c] |
| $S_0$ | 0.0 | 0.0 | | 6.152 | | 0.909(closed shell) |
| $S_1$ | 4.956 | 3.883 | 3.998[d] | 6.636 | 0.006 | 0.693(1−2′) −0.500(2−1′) |
| $S_2$ | 6.258 | 4.294 | 4.402[e] | 13.290 | 0.450 | 0.826(1−1′) |

[a] The computational results are obtained by (12,11)CASSCF except for the MRMP2 column. [b] The values are given in the velocity form. [c] The CSFs of which absolute values of CASSCF coefficients are greater than 0.3 are listed. The six occupied $\pi$-orbitals and the lowest five unoccupied $\pi$*-ones in the order of energy are designated by 6,5,4,3,2(HOMO-1),1(HOMO),1′(LUMO),2′(LUMO+1),3′,4′,5′, respectively. 1−1′ in the parenthesis, for instance, indicates the CSF of single excitation from orbital 1 to 1′. [d] The value taken from 0−0 band in ref 23. [e] The value taken from absorption maximum in *n*-hexane in ref 9.

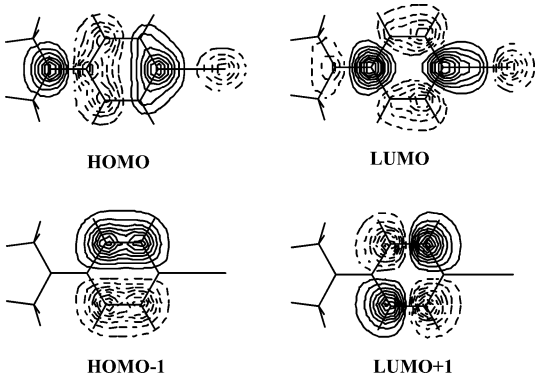


**Figure 2.** Molecular orbitals (MOs) relevant to $S_1$ and $S_2$ at $S_0$-geometry. The MOs are obtained by SA2-(12,11)CASSCF.

state functions (CSFs). In Figure 2, we show the relevant molecular orbitals (MOs) to see what types of excitations contribute to each excited state. As pointed out in previous calculations,[28,30,31] the $S_1$ and $S_2$ states are assigned to LE and CT, respectively. That is, the $S_1$ state with weak transition intensity from $S_0$ is well described by the excitations within the benzene ring. The $S_2$ state with strong transition intensity is well described by the HOMO−LUMO (HOMO; highest occupied MO, LUMO; lowest unoccupied MO) single excitation so that the electron is transferred from the dimethylamino into the remaining parts. The excitation energies by MRMP2 well reproduce the experimental ones.

Next we discuss the optimized geometry around the FC region. In Table 2, we listed the characteristic optimized parameters of $S_0$-geometry as well as other important electronic states and conformations. The $S_0$-geometry is optimized to have $C_s$ symmetry (i.e., $\tau = 0.0°$) substantially. The wagging angle $\omega$ is 32.2° so as to take a nonplanar structure around the dimethylamino group. The N−C bond distance (1.399 Å) is somewhat shorter than a normal C−N single bond. This is due to resonance between the dimethylamino part and the adjacent benzene ring. The C−C bond distances in the benzene ring (ca. 1.40 Å) take the typical value of aromatic benzene. The stable geometry in $S_1$(LE-geometry), assigned to LE around the FC region, is optimized to have no symmetry, where the wagging angle is 35.9°, the torsional angle is 36.4° (not 0°). This torsional angle is not so different from the experimental estimation (26.2°).[23] Another characteristic point is that the bond distances in the benzene ring are longer by ca. 0.04 Å, which is similar to previous study.[25] As pointed out in the LE states of the $\pi$ conjugated molecules with benzene ring,[37−39] an enlargement of the benzene ring(s) can be interpreted in terms of the nature of relevant MOs (see Figure 2). That is, the electron is excited from the occupied $\pi$ into an unoccupied $\pi$* orbital so as to weaken the skeletal benzene ring. We did additional optimization in $S_1$ under constraint of $C_s$ symmetry (LE($C_s$)-geometry). Except for $\tau$, the optimized parameters in $S_1$ at LE($C_s$)-geometry are very similar to those at LE-geometry. From the viewpoint of energy, the $S_1$ state at LE($C_s$)-geometry is more unstable only by 0.020 eV than that at LE-geometry. This energy difference is similar to the experimental estimation of the $\tau$-torsional barrier of 0.024 eV (i.e., 190 $cm^{-1}$).[23] The large difference between the experiment and calculation is about the wagging angle. From the experiment, the wagging angle $\omega$ is estimated to be 0°, whereas it is a nonzero value of 35.9° in our present calculation. So we optimized the geometry of LE under constraint of $C_2$ symmetry (LE($C_2$)-geometry). As seen in Table 2, the characteristic optimized parameters at LE- and LE($C_2$)-geometries are not so different from each other except for the wagging angle. The energy difference between them (i.e., inversion barrier) is only 0.041 eV. Taken into account that both the torsional and inversion energy barriers are small, the potential energy surface in $S_1$ with LE character has 2-fold double wells with respect to $\omega$ as well as $\tau$ but the wagging and torsional motions in $S_1$ around LE-geometry are very floppy.

As to the stable geometry in $S_2$ attributable to the CT state, we cannot find it in the FC region. Instead we carried out the optimization under constraint of $C_{2v}$ (CT($C_{2v}$,0)-geometry). The

**TABLE 2: Characteristic Optimized Parameters of DMABN[a]**

| geometry | $S_0$ | LE | LE($C_s$) | LE($C_2$) | LE($C_{2v}$,0) | LE($C_{2v}$,90) | CT | CT($C_{2v}$,0) | CT($C_{2v}$,90) | $S_2/S_1$−CIX |
|---|---|---|---|---|---|---|---|---|---|---|
| | | | | | Bond Distances (Å) | | | | | |
| $R$($C^1$—$C^2$) | 1.400 | 1.438 | 1.434 | 1.433 | 1.433 | 1.442 | 1.438 | 1.447 | 1.438 | 1.442 |
| $R$($C^2$—$C^3$) | 1.394 | 1.433 | 1.435 | 1.435 | 1.435 | 1.437 | 1.374 | 1.388 | 1.374 | 1.406 |
| $R$($C^3$—$C^4$) | 1.413 | 1.442 | 1.441 | 1.439 | 1.440 | 1.440 | 1.433 | 1.438 | 1.433 | 1.449 |
| $R$($C^4$—$C^5$) | 1.413 | 1.438 | 1.441 | 1.439 | 1.440 | 1.440 | 1.433 | 1.438 | 1.433 | 1.445 |
| $R$($C^5$—$C^6$) | 1.394 | 1.438 | 1.435 | 1.435 | 1.435 | 1.437 | 1.374 | 1.388 | 1.374 | 1.406 |
| $R$($C^6$—$C^1$) | 1.400 | 1.437 | 1.434 | 1.433 | 1.433 | 1.442 | 1.437 | 1.447 | 1.438 | 1.444 |
| $R$(N—$C^4$) | 1.399 | 1.403 | 1.385 | 1.373 | 1.372 | 1.406 | 1.438 | 1.400 | 1.438 | 1.408 |
| $R$($C^1$—$C^\alpha$) | 1.449 | 1.434 | 1.436 | 1.438 | 1.437 | 1.431 | 1.426 | 1.414 | 1.426 | 1.430 |
| $R$($C^\alpha$≡N) | 1.164 | 1.167 | 1.167 | 1.167 | 1.167 | 1.167 | 1.170 | 1.176 | 1.170 | 1.144 |
| | | | | | Torsional Angle (deg)[b] | | | | | |
| $\tau$ | 0.0 | 36.4 | 0.0 | 22.3 | 0.0 | 0.0 | 90.0 | 0.0 | 90.0 | 90.0 |
| | | | | | Wagging Angle (deg)[c] | | | | | |
| $\omega$ | 32.2 | 35.9 | 25.6 | 0.0 | 0.0 | 0.0 | 7.2 | 0.0 | 0.0 | 19.7 |

[a] The parameters are obtained by a state specific (12,11)CASSCF, though those at $S_2/S_1$−CIX is by SA2-(8,7) CASSCF as mentioned in the text. [b] The torsional angle $\tau$ of DMABN is defined in Figure 1. [c] The wagging angle $\omega$ is calculated by the inner product between **r**($C^4$—N) and the bisector vector of $\angle C^aNC^b$.

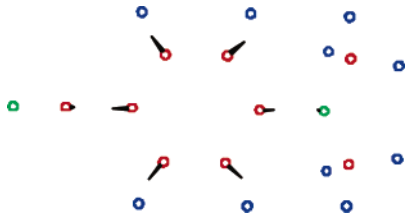

**Figure 3.** Force acting on each atom in $S_1$ at $S_0$-geometry by means of $S_1$-specific (12,11)CASSCF.

CT($C_{2v}$,0)-geometry is characterized by a quinoid structure where the aromaticity of the benzene ring disappears. That is, the bond distances of $C^2-C^3$ and $C^5-C^6$ become shorter than those in $S_0$ and the other bonds in the benzene ring become longer. We will refer to the quinoid structure in relation to the photochemical behavior after the main transition of $S_0-S_2$.

Now we discuss the photochemical behavior after electronic excitation. In this paragraph, we focus on a fate after the weak $S_0-S_1$ transition. As mentioned above, the $S_1$ state around the FC region is assigned to the LE state of which geometry is characterized by an enlarged benzene ring. In Figure 3, we show the force acting on each atom in $S_1$ at $S_0$-geometry. It can be seen that DMABN tends to enlarge a size of the benzene ring so as to directly relax into the stable LE-geometry in $S_1$. Finally, DMABN relaxes into $S_0$ through emission from $S_1$. The energy difference between $S_0$ and $S_1$ at LE-geometry (i.e., 3.681 eV by MRMP2 correction) is in good agreement with the experimental fluorescence maximum assigned to the emission from LE (3.633 eV).[9]

In turn, we discuss the photochemical behavior after the strong transition of $S_0-S_2$. As mentioned above, the $S_2$ state is assigned to CT with a large dipole moment but no stable geometry in $S_2$ under $C_1$ symmetry is found around the FC region. We tried to search a globally stable geometry in $S_2$ away from the FC region so as to fail in the optimization. This is because $S_2$ is very close to $S_1$ at a given geometry in optimization step by means of $S_2$-specific (12,11)CASSCF method. This implies that there is no stable geometry in $S_2$ or only the crossing region between $S_2$ and $S_1$ (i.e., $S_2/S_1-$CIX) where the radiationless relaxation takes place. Then we searched the $S_2/S_1-$CIX. In determination of $S_2/S_1-$CIX, we reduce computational labor in the following two ways. Because we experienced that determination of CIX for a similar size of molecule is much more computational demanding than those of stable geometry or saddle point. One is the reduction of the active space. In the scanning of the potential energy surfaces, it is found that both $S_1$ and $S_2$ states in our present interest are well described by the four highest occupied orbitals and the lowest three unoccupied orbitals. That is, (8,7)CASSCF is proper to determine $S_2/S_1-$CIX. The other is that the basis set for the benzene ring reduces from DZ + polarization into DZ quality. After the determination of $S_2/S_1-$CIX by SA2-(8,7)CASSCF, we checked if these reductions are valid for $S_2/S_1-$CIX with the original basis set mentioned in section 2. In Table 3, we listed the electronic structures at $S_2/S_1-$CIX by means of our present standard SA2-(12,11)CASSCF in the evaluation of potential energy of $S_1$ and $S_2$. The energy difference is small enough to be a CIX even by a larger scale calculation of SA2-(12,11)CASSCF with the original basis set. This implies that SA2-(12,11)CASSCF, which is practically prohibited, gives a similar result by the present SA2-(8,7)CASSCF with a smaller basis set. Judging from the dipole moments, $S_2/S_1-$CIX is a crossing region between the CT and LE states. From the main CSFs and the relevant MOs in Figure 4, the electron is found

**TABLE 3: Energies, Dipole Moments, and the Main CSFs of DMABN at $S_2/S_1$-CIX by Means of SA2-(12,11)CASSCF Method**

| | energy (eV)[a] | dipole moment (Debye) | main CSFs[b] |
|---|---|---|---|
| $S_1$ | 5.421 | 3.866 | 0.568(1−2′) +0.621(2−1′) |
| $S_2$ | 5.600 | 15.148 | 0.886(3−1′) |

[a] The energy is relative to that at $S_0$-geometry. [b] The CSFs of which absolute values of CASSCF coefficients are greater than 0.3 are listed. The six occupied $\pi$-orbitals and the lowest five unoccupied $\pi^*$-ones in the order of energy are designated by 6,5,4,3(HOMO-2),2(HOMO-1),1(HOMO),1′(LUMO),2′(LUMO+1),3′,4′,5′, respectively. 1−1′ in the parentheses, for instance, indicates the CSF of single excitation from orbital 1 to 1′.

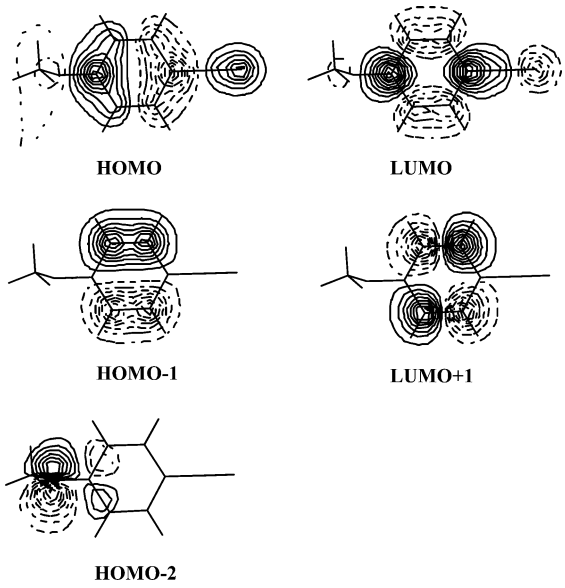


**Figure 4.** MOs relevant to $S_1$ and $S_2$ at $S_2/S_1-$CIX. The MOs are obtained by SA2-(12,11)CASSCF at $S_2/S_1-$CIX.

to be transferred from the dimethylamino into the remaining parts in the CT state, whereas the LE state is locally excited within the benzene ring. The optimized geometry at $S_2/S_1-$CIX is listed in Table 2. The characteristic point is that the torsional angle $\tau$ is 90°. Another is that the $C^1-C^2$, $C^6-C^1$, $C^3-C^4$, and $C^4-C^5$ bond distances become longer, whereas the $C^2-C^3$ and $C^5-C^6$ bond distances are not so different from those in $S_0$-geometry. In other words, the benzene skeleton is characterized by a quinoid structure where the aromaticity of the benzene ring disappears. So our concern is how DMABN in $S_2$ at $S_0$-geometry reaches into $S_2/S_1-$CIX. In Figure 5, we show two types of potential energy curves with respect to $\tau$ by means of SA2-(12,11)CASSCF. One is obtained as a variable of $\tau$ with the other geometrical parameters fixed to those of $S_0$-geometry. The other is obtained as a function of $\tau$ where the other geometrical parameters are fixed to those of $S_2/S_1-$CIX. From these figures, it is found that both $S_2$ energies become lower as an increment of $\tau$. This means that the curvature of potential energy surface with respect to $\tau$ suddenly changes from a positive to a negative value upon electronic transition of $S_0-S_2$ Consequently, the zero point vibration with respect to $\tau$ in $S_0$ serves to promote the torsional motion in $S_2$ so that DMABN in $S_2$ can easily leave the FC region and reach into $S_2/S_1-$CIX. Here we have another question, when does DMABN in $S_2$ lose its aromaticity of the benzene ring on the way from aromatic $S_0$-geometry into quinoid $S_2/S_1-$CIX? There are three possible pathways. Path I: A quinoid structure is first formed in the FC

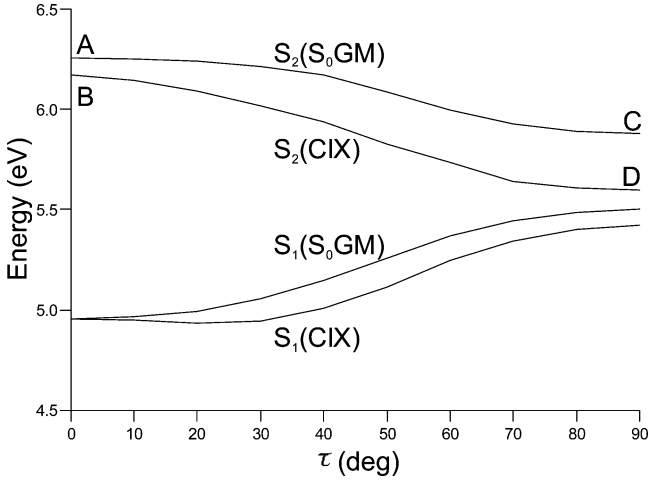


**Figure 5.** Potential energy curves with respect to $\tau$ by SA2-(12,11)-CASSCF. The potential energy curve of $S_1(S_0GM)$ is, for instance, obtained by varying $\tau$ where the other parameters are fixed to those at $S_0$-geometry. The $S_2(CIX)$ is the $S_2$ curve where the other parameters are fixed to those of $S_2/S_1-CIX$. The energies are relative to $S_0$ at $S_0$-geometry. The points of A,B,C and D are referred in the text.


**Figure 6.** Force acting on each atom in $S_2$ at $S_0$-geometry by means of $S_2$-specific (12,11)CASSCF.

region and then the torsional motion takes place so as to reach into $S_2/S_1-CIX$. Path II: The torsional motion first takes place to exit from the FC region and then the aromaticity of the benzene ring is lost at highly $\tau$-twisted region. Path III: Both events take place simultaneously. Roughly speaking, these correspond to the pathways of A → B → D, A → C → D, and A → D in Figure 5, respectively. As to path I, we think that it is unrealistic for the following reason. Path I implies that the $\tau$-torsional motion is suppressed until the aromatic benzene ring changes into a quinoid structure around the FC region. As deduced from the above discussion, however, the curvature of the $S_2$ potential energy surface with respect to $\tau$ is negative around the FC region so that DMABN can immediately exit from the FC region through the $\tau$-torsional motion upon electronic excitation. Therefore, path I, A → B → D, seems to be unrealistic. Path II , A → C → D, also seems to be unrealistic for the following reason. In Figure 6, we show the force acting on each atom in $S_2$ at $S_0$-geometry. It can be seen that DMABN tends to form a quinoid structure right after electronic excitation into $S_2$. From the side view, it is also found that the dimethyl-amino group tends to change from a pyramidal into a planar structure. However, the $\tau$-torsional motion is impossible to suppress upon electronic excitation, as noted above. Therefore, we conclude that path III is the most realistic. That is, both the $\tau$-torsional motion and the loss of the aromaticity of the benzene ring take place simultaneously to reach into $S_2/S_1-CIX$ from the FC region. To check the above discussion further, a molecular dynamic simulation on the $S_2$ surface, of which starting points are properly sampled around the $S_0$-geomtry, is desirable.

The next concern is the fate of DMABN in $S_1$ after relaxation at $S_2/S_1-CIX$. To examine it, we pursued the forward and

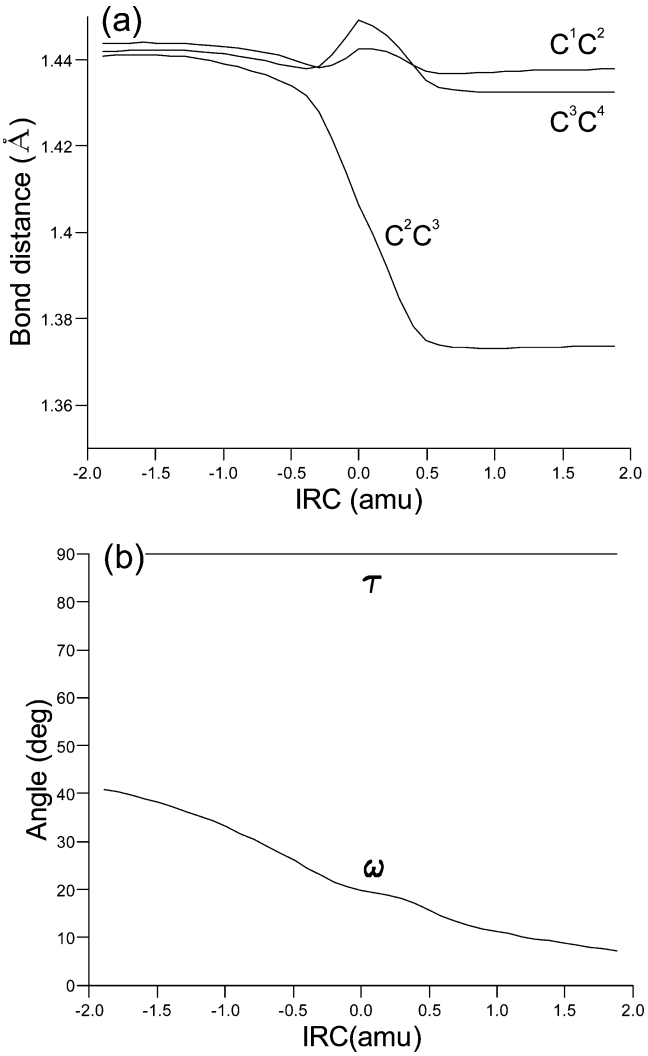


**Figure 7.** Characteristic geometrical parameters along the reaction coordinate, which is obtained by an $S_1$-specific (12,11)CASSCF. (a) The bond distances in the benzene ring. The bond distances of $C^1C^6$, $C^5C^6$, and $C^4C^5$, not drawn, are very similar to those of $C^1C^2$, $C^2C^3$, and $C^3C^4$, respectively. (b) The torsional ($\tau$) and wagging ($\omega$) angles.

backward reaction coordinate in $S_1$ from $S_2/S_1-CIX$. In Figure 7, we show the characteristic geometrical parameters as a function of reaction coordinate. As to the bond distances of the benzene ring (see Figure 7a), the $C^2-C^3$ and $C^5-C^6$ largely change in the vicinity of $S_2/S_1-CIX$. In the negative value of the reaction coordinate (i.e., the backward reaction), all the six bond distances of the benzene skeleton converge to ca. 1.44 Å. That is, the backward reaction is expected to finally reach into LE-geometry (refer to Table 2), which is characterized by an enlarged benzene ring, though we followed the backward reaction coordinate up to only 2 amu in the present calculation. On the other hand, in the positive value (i.e., the forward reaction), the $C^2-C^3$ and $C^5-C^6$ bond distances become shorter so as for a quinoid character to increase. In other words, in the forward reaction, DMABN goes to the other product of the CT state in $S_1$. In Table 2, we listed the optimized geometrical parameters of the CT state in $S_1$ (CT-geometry). In comparison of CT-geometry with $S_2/S_1-CIX$, a contribution of the quinoid structure at CT-geometry increases; i.e., the $C^2-C^3$ and $C^5-C^6$ bond distances become shorter, and the other bond distances in the benzene skeleton remain unchanged at 1.43−1.44 Å. As to the torsional and wagging angles (see Figure 7b), we can also find another interesting point. It can be seen that the

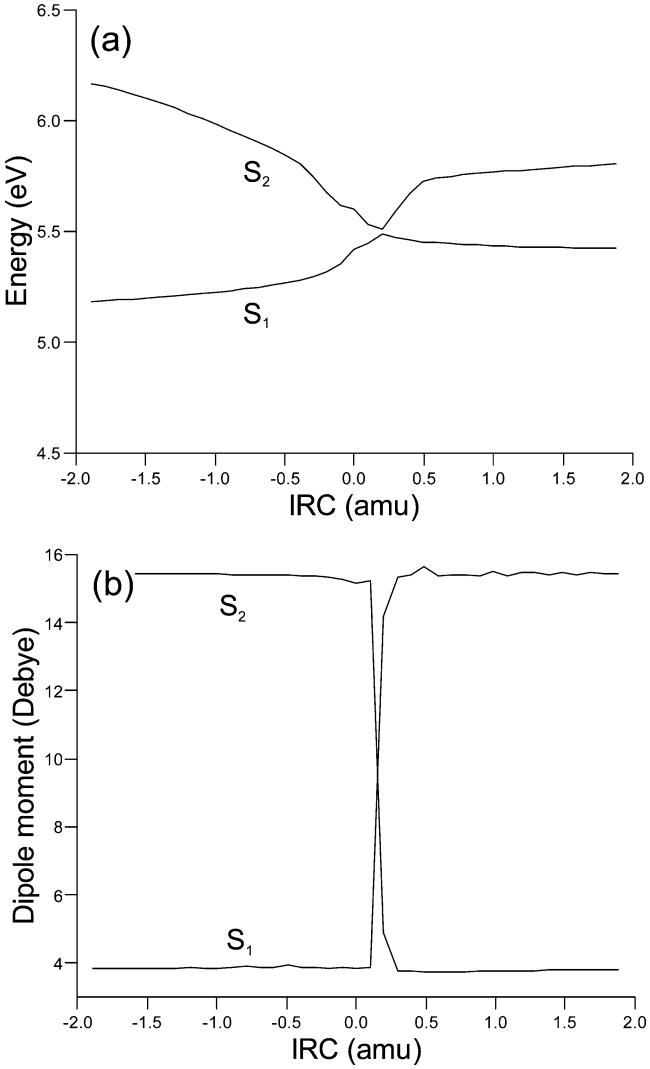


**Figure 8.** (a) Energy profile and (b) dipole moments along the reaction coordinate by SA2-(12,11)CASSCF. The energies are relative to that in $S_0$ at $S_0$-geometry.

torsional angle is almost constant to 90° around the $S_2/S_1-$CIX, whereas the wagging angle largely changes. In the backward reaction, the wagging angle increases so as to be closer to that of LE-geometry. However, the torsional angle little changes from 90° at $S_2/S_1-$CIX. This means that the $\tau$-torsional motion back to LE-geometry is less important until other parameters, such as the bond distances, the wagging angle, are similar to those of LE-geometry. This finding is similar to the computational finding of the photoisomerization of styrene.[40] In the forward region, it decreases so as to take a more planar structure around the dimethylamino group. The $\tau$-torsional angle is also almost constant to 90°, as found in the backward region. Considering that the torsional angle at CT-geometry is also 90° (see Table 2), it is found that the potential surface of $S_1$ with respect to $\tau$ has a minimum at ca. 90° all the way from $S_2/S_1-$CIX to CT-geometry. Therefore, we conclude that the CT state is TICT even in the gas phase (or nonpolar solvent). As to the electronic structure, it is interesting to discuss the photochemical behavior of DMABN around the $S_2/S_1-$CIX. In Figure 8, we show the potential energy curves and the dipole moments as a function of the reaction coordinate. The dipole moments are a good measure to characterize the electronic structures. The CT state has a large dipole moment (ca. 15 D), whereas the LE state has a small one (ca. 4 D). So it is found that, in the backward region, $S_1$ can be assigned to LE, and $S_1$ is the CT state in the forward region. From the viewpoint of the potential energies, $S_1$ is not so energetically stabilized in the forward region, whereas $S_1$ is stabilized in the backward region. This implies the following. At $S_2/S_1-$CIX, DMABN is possible to go into both the LE and CT region. In the case of the branch into LE region, DMABN can easily escape from $S_2/S_1-$CIX into LE-geometry because the $S_1$ energy is quickly lowered. In the case of the branch into CT region, on the other hand, DMABN is not stabilized so as to return from CT region into $S_2/S_1-$CIX and further to pass over $S_2/S_1-$CIX into LE region.

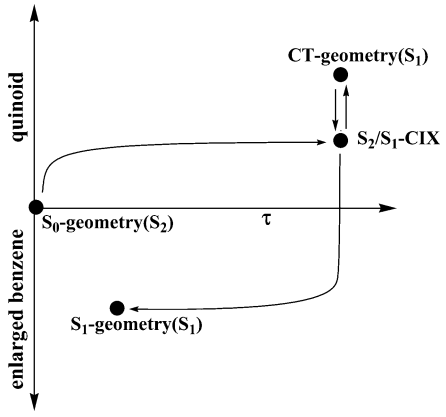


**Figure 9.** Schematic representation of the photochemistry of DMABN in gas phase (or nonpolar solvent) after the $S_0-S_2$ transition.

On the basis of the above discussion, we summarize a picture of the photochemical behavior of DMABN after the strong transition of $S_0-S_2$ in gas phase or nonpolar solvent, which is schematically shown in Figure 9. In this figure, we newly define three coordinates to make it easy to understand the photoprocess of DMABN. The "quinoid" coordinate in the upper ordinate represents how much degree the aromaticity of the benzene ring is lost. The "enlarged benzene" in the lower ordinate represents how much the benzene ring expands with hexagon. The abscissa represents the torsional angle $\tau$. Right after electronic excitation into $S_2$, DMABN at $S_0$-geometry changes the $\tau$-torsional angle and lose its aromaticity of the benzene ring simultaneously so as to reach $S_2/S_1-$CIX characterized as a quinoid structure with the perpendicularly twisted dimethylamino group. At $S_2/S_1-$CIX, DMABN is possible to branch into the LE state as well as CT in $S_1$. DMABN branching into the LE state recovers the aromaticity and expands the benzene ring almost keeping perpendicularly twisted conformation and then relaxes into the stable geometry of LE-geometry in $S_1$ through the $\tau$-torsional motion. DMABN branching into the CT state has more quinoid character where the dimethylamino group remains perpendicularly twisted. However, CT-geometry is not energetically stabilized in gas phase or nonpolar solvent so that DMABN in the CT region it easily passes over $S_2/S_1-$CIX and finally relaxes into the most stable LE-geometry in $S_1$. This is an explanation for why only the fluorescence from LE state is observed in gas phase and nonpolar solvent, irrespective of excitation energies.

Next we discuss the photochemical behavior of DMABN in a polar solvent. In a conventional TICT picture, the CT state in $S_2$ becomes stable as the $\tau$-torsional angle increases, whereas the LE state in $S_1$ becomes unstable. At a given torsional angle, two surfaces cross so that two species of LE and CT are possible to interconvert with each other. In a polar solvent, the CT state is more stabilized than the LE state. Consequently, the CT (i.e., TICT) state is much more populated so that only the emission from the CT state is observed. In this picture, it is implicitly

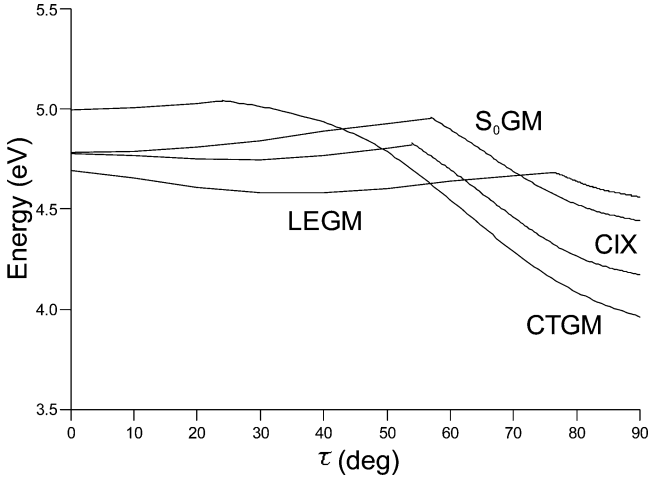


**Figure 10.** Free energy curves in $S_1$ with respect to $\tau$ by a state-specific (12,11)CASSCF. The other parameters are fixed to those at $S_0$-geometry($S_0$GM), LE-geometry(LEGM), $S_2/S_1$-CIX(CIX), and CT-geometry(CTGM), respectively. The free energies are relative to that in $S_0$ at $S_0$-geometry.

assumed that the torsional motion takes place on a similar time scale of solvent reorganization (at least 1 ps). However, Fuss et al. reported a very interesting finding that this implicit assumption is doubtful.[27] They found that the torsional motion after excitation into $S_2$ is very fast (68 fs) to reach into $S_2/S_1-$CIX. Their experimental finding forces us to revise the conventional picture mentioned above. In the initial stage (less than 100 fs) when the reorganization of the surrounding solvent molecules is not allowed to follow the change of the electronic structure into CT, the internal conversion from $S_2$ into $S_1$ at $S_2/S_1-$CIX is completed. Then the equilibration process between LE and CT, which is experimentally estimated to be on a time scale of 3−4 ps,[7,18] takes only on the $S_1$ surface. Therefore, we revise the conventional picture into the following. The equilibration process between LE and CT only represents a dynamics on a time scale of picoseconds in polar solvent, whereas on a shorter time scale of less than 100 fs, electronically excited DMABN through $S_0-S_2$ transition relaxes into $S_1$ at $S_2/S_1-$CIX with little effect of solvent polarity.

To examine the dynamics on a time scale of picoseconds in more detail, we calculated the free energy in $S_1$, where we used a state-specific (12,11)CASSCF combined with PCM method. The torsional angle $\tau$ is a good coordinate to see the picosecond-order dynamics. In Figure 10, we show the free energy curves of $S_1$ in typical aprotic polar solvent of dimethyl sulfoxide (DMSO) with respect to $\tau$ where the other parameters are fixed to $S_0$-, LE-, and CT-geometries and $S_2/S_1-$CIX. All four free energy curves have cusps at nonperpendicularly twisted angles

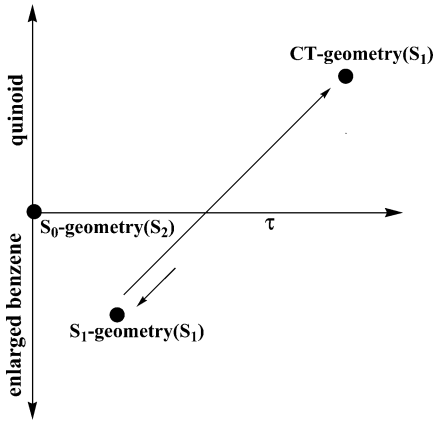


**Figure 11.** Schematic representation of the photochemistry of DMABN in $S_1$ in polar solvent on a timescale of several picoseconds and longer.

(i.e., 76° for "LEGM", 57° for "$S_0$GM", 54° for "CIX", 24° for "CTGM", respectively). This is because the electronic structure in $S_1$ switches at each cusp. At a smaller torsional angle, each $S_1$ has LE character, but it has CT character at a larger torsional angle, judging from the large electrostatic interaction energy. In the LE state at a smaller torsional angle, the "LEGM" state is the most energetically stable and its minimum with respect to $\tau$ is similar to that at LE-geometry in the gas phase. At a larger torsional angle, on the other hand, the "CTGM" state is the most stable. Furthermore, it is found that the order among the free energies at highly twisted region is $F_1$(CTGM) < $F_1$(CIX) < $F_1$($S_0$GM) < $F_1$(LEGM). Considering that the CT-geometry (and $S_2/S_1-$CIX) is characterized by a quinoid structure, we can conclude that a loss of the aromaticity of the benzene ring is an essential factor for the CT formation in polar solvent as well as the dimethylamino perpendicularly twisted structure. Actually, a quinoid structure with CT character is observed in the polar solvent by means of picosecond time-resolved spectroscopic experiments.[18,19,26] On a time scale of several picoseconds and longer, LE- and CT-geometries are equilibrated in polar solvent so that the more stable CT species in polar solvent are populated more and finally emit a fluorescence from the CT-geometry, which is schematically represented in Figure 11.

As mentioned in the Introduction, the geometrical structure of the CT state in polar solvent has been long controversial. Recently, Zachariasse and co-workers reported the photochemistry of several rigid DMABN related molecules that are prevented from the torsional motion, to validate their PICT model.[12] In Table 4, we listed the emission properties in nonpolar solvent, the energy gaps between $S_1$ and $S_2$, and the dipole moments of $S_1$ and $S_2$ at the equilibrium geometries in

**TABLE 4: Emission Properties in Nonpolar Solvent, Energy Gaps between $S_1$ and $S_2$, and Their Dipole Moments of DMABN Derivatives at the $S_0$-Optimized Geometries[a]**

| molecule | emission properties[b] (in *n*-hexane) | $S_2-S_1$ energy gap (eV)[c] | dipole moment (Debye) | |
|---|---|---|---|---|
| | | | $S_1$ | $S_2$ |
| DMABN | LE | 1.219 | 7.117 | 13.225 |
| NMC5 | LE | 1.244 | 6.317 | 12.673 |
| NMC6 | LE | 1.148 | 6.800 | 13.228 |
| NTC5 | LE | 1.083 | 7.082 | 13.372 |
| NTC6 | CT + LE | 0.934 | 7.039 | 13.916 |
| NTCM6 | CT (expected) | 0.851 | 7.234 | 14.116 |
| TMABN | CT | 0.576 | 4.115 | 15.283 |
| BMABN | CT + LE (minor) | 0.498 | 4.380 | 15.263 |

[a] All the $S_0$-optimized geometries are obtained by restricted Hartree−Fock calculations and so the values for DMABN are slightly different from those in Table 1. [b] The emission properties taken from refs 6 (for TMABN) and 12 (for others). [c] The $S_2-S_1$ energy gap is evaluated by SA2-(12,11)CASSCF method.

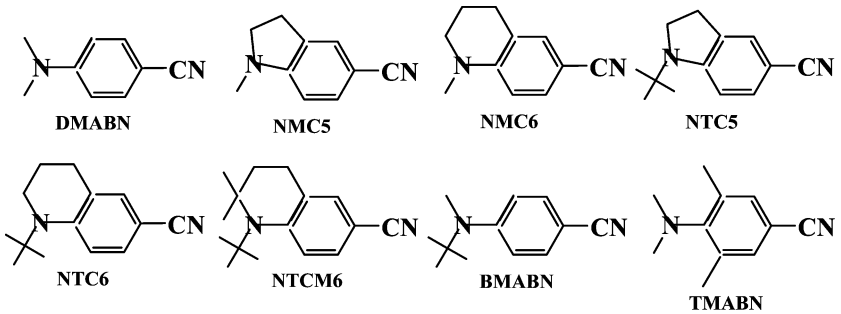


**Figure 12.** Chemical structures of DMABN derivatives and their abbreviations: DMABN, 4-(dimethylamino)benzonitrile; NMC5, 1-methyl-5-cyanoindoline; NMC6, ethyl-6-cyanotetrahydroquinoline; NTC5, 1-*tert*-butyl-5-cyanoindoline; NTC6, 1-*tert*-butyl-6-cyanotetrahydroquinoline; NTCM6, 1-*tert*-butyl-6-cyano-2,2-dimethyltetrahydroquinoline; BMABN, 4-(*tert*-butylmethylamino)benzonitrile; TMABN, 4-(dimethylamino)-3,5-dimethylbenzonitrile.

**TABLE 5: Characteristic Optimized Parameters of DMABN Derivatives**

| molecules | DMABN[a] | NMC5 | NMC6 | NTC5 | NTC6 | NTCM6 | TMABN | BMABN |
|---|---|---|---|---|---|---|---|---|
| | | | | Bond Distances (Å) | | | | |
| $R(C^1-C^2)$ | 1.393 | 1.405 | 1.400 | 1.403 | 1.397 | 1.394 | 1.387 | 1.393 |
| $R(C^2-C^3)$ | 1.381 | 1.370 | 1.376 | 1.369 | 1.378 | 1.379 | 1.392 | 1.385 |
| $R(C^3-C^4)$ | 1.410 | 1.404 | 1.414 | 1.409 | 1.416 | 1.416 | 1.404 | 1.395 |
| $R(C^4-C^5)$ | 1.410 | 1.389 | 1.399 | 1.395 | 1.400 | 1.405 | 1.407 | 1.398 |
| $R(C^5-C^6)$ | 1.381 | 1.392 | 1.388 | 1.391 | 1.387 | 1.385 | 1.388 | 1.386 |
| $R(C^6-C^1)$ | 1.393 | 1.390 | 1.387 | 1.388 | 1.386 | 1.386 | 1.390 | 1.392 |
| $R(N-C^4)$ | 1.380 | 1.388 | 1.385 | 1.392 | 1.399 | 1.410 | 1.429 | 1.430 |
| $R(C^1-C^\alpha)$ | 1.445 | 1.446 | 1.445 | 1.445 | 1.446 | 1.445 | 1.450 | 1.449 |
| $R(C^\alpha\equiv N)$ | 1.141 | 1.141 | 1.141 | 1.141 | 1.141 | 1.141 | 1.140 | 1.140 |
| | | | | Torsional Angle (deg)[b] | | | | |
| $\tau$ | 0.0 | −2.8 | 19.6 | −6.9 | 32.1 | 30.8 | 79.2 | −107.5 |
| | | | | Wagging Angle (deg)[c] | | | | |
| $\omega$ | 24.4 | 40.8 | 26.3 | 32.4 | 19.5 | 11.2 | 33.3 | 39.1 |

[a] All the $S_0$-optimized geometries are obtained by restricted Hartree−Fock calculations and so the values for DMABN are slightly different from those in Table 2. [b] The definitions of the torsional angles $\tau$ of DMABN derivatives are similar to that of DMABN in Figure 1. [c] The definitions of the wagging angles $\omega$ are similar to that of DMABN in the caption in Table 2.

$S_0$ about DMABN and related molecules (refer to Figure 12 for the chemical structures and their abbreviations). Judging from the dipole moments, $S_1$ and $S_2$ of all the DMABN derivatives studied here can be assigned to LE and CT, respectively. However, the energy gap depends on the substituent. As to the first five molecules in Table 4 (i.e., DMABN, NMC5, NMC6, NTC5, and NTC6) of which emission properties were examined by Zachariasse et al., the followings are found: (i) the energy gap of the rigidized six-membered ring molecule is smaller than that of the corresponding five-membered ring molecule; (ii) the *tert*-butyl group serves to decrease the energy gap much more than the methyl group. We further examined the substituent effect in relation to $S_0$-geometry (hereafter, we also call the $S_0$-equilibrium geometry of DMABN derivatives $S_0$-geometry besides $S_0$-geometry of DMABN). In Table 5, we listed the characteristic parameters at $S_0$-geometry. Though each bond distance is similar irrespective of molecules, the torsional ($\tau$) and the wagging ($\omega$) angles are strongly dependent on molecules. Contrary to the fact that the amino groups of five-membered ring molecules of NMC5, NTC5, and DMABN are nontwisted, those of six-membered ring molecules of NMC6 and NTC6 are pretwisted even at $S_0$-geometry. This implies that the $S_2/S_1$−CIXs of NMC6 and NTC6 are located near $S_0$-geometry. In other words, the energy gaps of these six-membered DMABN derivatives at $S_0$-geometries are smaller than those of five-membered DMABN derivatives and DMABN itself. As to the wagging angles, we can find out another relationship between geometry and energy gap. The bulky *tert*-butyl group serves for the amino group to take more planar structure (i.e., smaller wagging angle). To avoid the steric repulsion between the bulky *tert*-butyl group and the benzene ring, there are two ways for conformational relaxation in $S_0$. One is that the amino group is twisted though $\tau$-tosional motion, from which the rigid molecules are prevented. The other is that the wagging angle decreases so the *tert*-butyl group is located further away from the benzene ring. As mentioned above, a planar structure around the amino group favors a CT state. This causes the $S_2$ state with CT character to become energetically lower at $S_0$-geometry and consequently the energy gap becomes smaller. By virtue of the above two factors, the energy gap of NTC6 is smallest of the first five molecules (in Table 4) that were examined by Zachariasse and co-workers. Therefore, only NTC6 of the first five molecules in Table 4 has the CT emission property even in nonpolar solvent. If we apply this principle to NTCM6, which are more crowded around the amino group, the energy gap is expected to be smaller than that of NTC6 due to the smaller wagging angle. In Tables 4 and 5, our predictions are found to be right. Furthermore, we apply this principle to another molecule of TMABN and BMABN. In the former case of TMABN, the amino group is highly pretwisted even in $S_0$-geomtry due to the steric hindrance between dimethylamino group and methyl ones bonded to the benzene ring. In the latter case of BMABN, it is also highly pretwisted due to the steric repulsion between the bulky *tert*-butyl group and the benzene ring. Therefore, both energy gaps of the molecules are expected to be small. Actually, in both cases, CT emission is observed even in nonpolar solvent.[10,12]

We mention the CT emission property in relation with TICT and PICT models. To do this, we begin with the comment on the relationship between these models and geometrical parameters of $\tau$ and $\omega$. The TICT model is related to the torsional angle of $\tau$, whereas the PICT model is related to the wagging

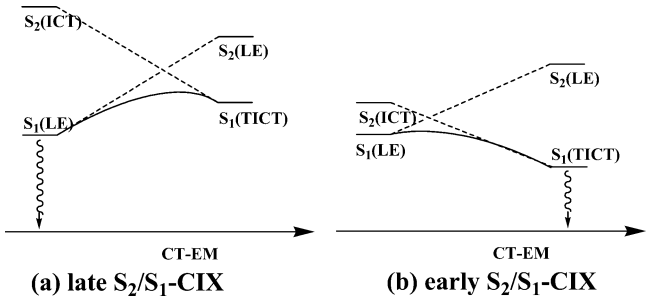


**Figure 13.** Schematic representation of the relationship between emission properties and the position of $S_2/S_1$-CIX: (a) late $S_2/S_1$-CIX for the LE emission; (b) early $S_2/S_1$-CIX for the CT emission. The comment on the words of "late" and "early" as well as the meaning of the "CT-EM" coordinate are made in the text.

angle of $\omega$, leading to a planar quinoid structure. So NTC6 with a small $\omega$, which is prevented from a large $\tau$-torsion, is a typical example to validate the PICT model. On the other hand, TMABN with a large $\tau$ is a typical example for TICT. However, as far as looking into the energy gap, which is a guiding principle for the PICT model, TMABN also seems to be a good example for PICT model! This contradiction implies the following. "Which of TICT or PICT is correct?" is a meaningless question, or both TICT and PICT models have advantage and disadvantage against the other to explain the emission property. To overcome disadvantage for each model, we propose a new and simple guiding principle about the emission property of DMABN derivatives in gas phase or nonpolar solvent. *A smaller wagging $\omega$ and/or larger torsional $\tau$ angle(s) in $S_0$-geometry leads to a better condition for the CT emission.* The essence of our new guiding principle is that the CT emission is determined by both $\tau$ and $\omega$, though it is determined by only one factor of $\tau$ or $\omega$ in conventional TICT and PICT models. In other words, in our new guiding principle, we are beyond the controversy between TICT and PICT and both models are properly incorporated with each other. With the aid of this principle, we can easily understand that both TMABN and NTC6 have CT emissive character, whereas DMABN has LE one. To give more insight into our new guiding principle, we mention it in relation with the shape of the potential energy surfaces, shown in Figure 13 schematically. In this figure, we introduce a new coordinate labeled as "CT-EM". The "CT-EM" is a measure of how much a geometry changes in favor of CT emission. So the left-hand side of figure corresponds to a stable geometry in LE state as well as $S_0$-geometry, whereas the right-hand side corresponds to a stable CT geometry. From the figures, it can be seen that the emission properties of LE and CT is determined by the position of $S_2/S_1-$CIX. In the case of the LE emission (see Figure 13a), $S_2/S_1-$CIX is located far away from $S_0$-geometry and the LE state is more stabilized than the CT state in $S_1$. Therefore, all the electronically excited species in $S_2$ is relaxed into the LE state in $S_1$ and finally emits fluorescence. In the case of CT emission (see Figure 13b), on the other hand, $S_2/S_1-$CIX is located in the neighborhood of $S_0$-geometry. This causes the opposite effect and finally CT fluorescence is observed. We can rephrase these explanations in other words that "early" and "late" $S_2/S_1-$CIXs relate to the CT and LE emission properties, respectively. Here we referred to the terms of "early" and "late" by analogy with a well-known Hammond postulate in organic chemistry.[41] Now we make more comment on the "CT-EM". So we consider the relationship between the position of $S_2/S_1-$CIX and the geometrical parameters of $\tau$ and $\omega$. As mentioned above, both TMABN and NTC6 have the CT emission property, commonly characterized

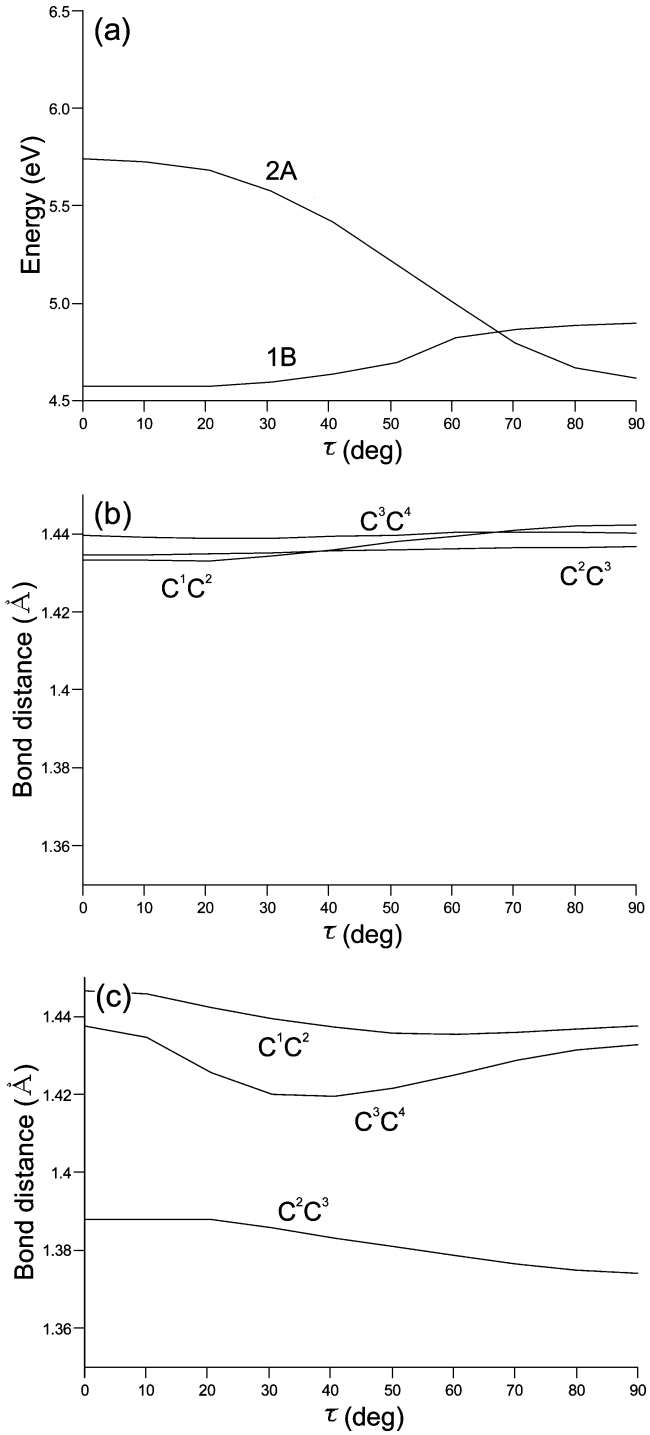


**Figure 14.** (a) Potential energy curves with respect to $\tau$. The other parameters are optimized for each $\tau$ under $C_2$ symmetry by means of a state-specific (12,11)CASSCF. The energies are relative to that in $S_0$ at $S_0$-geometry. The optimized parameters of the benzene ring for (b) 1B and (c) 2A.

by "early" $S_2/S_1-$CIX. However, the $S_2/S_1-$CIX positions of NTC6 and TMABN are determined by a different geometrical factor. In the case of TMABN, which is a typical example of TICT model, it is determined by the $\tau$-torsional angle. Because TMABN is pretwisted, $S_2/S_1-$CIX is possibly located in the neighborhood of $S_0$-geometry. In the case of NTC6 which is a typical example of PICT model, it is, in turn, mainly determined by the wagging angle. Because NTC6 is more planar around the amino group (i.e., smaller $\omega$), the energy gap is smaller and $S_2/S_1-$CIX is possibly located in the neighborhood of $S_0$-

**TABLE 6: Energies in LE and CT States at Important Conformations (eV)**

| geometry | $S_0$ | LE | CT | CT($C_{2v}$,0) | $S_2/S_1-$CIX | CIX70 |
|---|---|---|---|---|---|---|
| CASSCF | (4.956, 6.258)[a] | (4.774, 6.208) | (5.804, 5.422) | (4.912, 5.960) | (5.421, 5.600) | (5.344, 5.641) |
| MRMP2 | (3.883, 4.294) | (3.786,[b] 4.082) | (4.621, 3.357) | (3.693, 3.977) | (4.351, 3.558) | (4.181, 3.963) |
| $\Delta E_{corr}$[c] | (1.073, 1.964) | (0.988, 2.126) | (1.183, 2.065) | (1.219, 1.983) | (1.070, 2.042) | (1.163, 1.678) |

[a] The first and second values in the parentheses are the energies in LE and CT states, respectively. The energies are relative to that in $S_0$ at $S_0$-geometry. [b] The calculated fluorescence energy (3.681 eV) in the text is obtained by the energy in LE (i.e., 3.786 eV) relative to that in $S_0$ (0.105 eV) at LE-geometry. [c] $\Delta E_{corr}$ is the MRMP2 energetic correction evaluated by $E$(CASSCF) − $E$(MRMP2).

geometry. Considering these discussions and also the fact that $\omega$ is in close relation with a quinoid structure, we interpret "CT-EM" in Figure 13 as a generalized coordinate where two factors of $\tau$ and quinoid coordinates defined in Figure 9 are included. Using Figure 13, we can also explain the difference of the photochemistry between gas phase (or nonpolar) and polar solvent. In the case of the DMABN photochemistry, for instance, $S_2/S_1-$CIX is far away from the $S_0$-geomtry in gas phase (or nonpolar solvent) (refer to Figure 13a). In polar solvent, on the other hand, the electronic state with CT character is more stabilized so that $S_2/S_1-$CIX is closer to $S_0$-geometry (refer to Figure 13b). Therefore, we understand that the emissive property of DMABN is determined by the position of $S_2/S_1-$CIX which is dependent on solvent polarity.

The photochemistry of DMABN has been frequently discussed under $C_2$ symmetry because the LE (1B) and CT (2A) states belong to different symmetry under $C_2$. Recently, Rappoport and Furche reported the potential energy curves which were optimized at each torsional angle $\tau$ ($\xi$ in their paper) for each state, by means of TDDFT method.[24] These curves represent the minimum energy path for each state. In their comment, at $\xi = 52°$, two curves of 2A and 1B cross each other, which allows electronically excited DMABN to branched into CT and LE. However, we wonder if $\xi = 52°$ in their curves is an actual crossing point. As seen in Table 2, LE($C_{2v}$,0)- and LE($C_{2v}$,90)-geometries are similar to each other and characterized as an enlarged benzene ring. This implies that the optimized geometry of 1B is characterized as an enlarged benzene ring irrespective of $\tau$. As to CT($C_{2v}$,0)- and CT($C_{2v}$,90)-geometries in Table 2, the same discussion can be done. That is, the optimized geometry of 2A is characterized by a quinoid structure without aromaticity of the benzene ring. Therefore, we think the energies of 2A and 1B are same at $\xi = 52°$ but the geometries are quite different from each other in their calculation. To validate our discussion, we actually calculated the potential energy curves of 1B and 2A which are optimized at each $\tau$ by means of a state-specific (12,11) CASSCF. In Figure 14, we show the potential energy curves and the bond distances in the benzene rings. The present 1B and 2A curves by (12,11)-CASSCF method give a feature similar to those by Rappoport and Furche. That is, in the highly twisted region (i.e., $\tau = 67°$), the energies of 1B and 2A are close to each other (see Figure 14a). However, the bond distances in the benzene rings in 1B are almost constant irrespective of $\tau$ and characterized by an enlarged benzene ring (see Figure 14b). From the bond distances of 2A (see Figure 14c), the geometry in 2A is characterized as a quinoid structure. Therefore, we conclude that two surfaces do not cross at $\tau = 67°$ in our present calculation as well as $\xi = 52°$ by Rappoport and Furche, though we think they pinpointed the relationship between emission properties and the potential energy surfaces.

Finally, we give a perspective on the refinement of our present model where TICT and PICT models are incorporated properly. The present model is substantially built up by CASSCF calculations where the static electron correlations are included enough but the dynamic electron correlations not included. So it is worthwhile to comment on how our present model is changed by a more sophisticated method of MRMP2 where the dynamics electron correlations are also included. In Table 6, we listed the energies at important conformations by (12,11)-CASSCF and MRMP2 methods. As pointed above, the MRMP2 energies well reproduce the experimental one, such as the absorption (at $S_0$-geometry) and fluorescence (at LE-geometry) energies. Furthermore, it is found that the MRMP2 energetic corrections are almost constant of 1 for LE, and 2 eV for CT, respectively, irrespective of conformations. This implies that the global surfaces of LE and CT by MRMP2, which is terribly computational demanding, are similar to modified surfaces where the present CASSCF surfaces are shifted down by 1 (for LE) and 2 eV (for CT), respectively. Here we come up with a question if a modified CT surface is possible to cross with a modified LE one at small or nontwisted $\tau$ value. At CT($C_{2v}$,0)-geometry characterized as a nontwisted quinoid structure, the CT state is still above LE and the energy difference between CT and LE (0.284 eV) is not so different from that at $S_0$-geometry (0.411 eV). This means that an $S_2/S_1-$CIX is unlikely to be located around the nontwisted geometry even by a more sophisticated MRMP2 method. As seen in the MRMP2 energies at CIX70-geometry where the torsional angle $\tau$ is 70° and the other parameters are fixed to those at $S_2/S_1-$CIX by the present CASSCF method, the energy difference (0.218 eV) is small to be a CIX. This implies that, even in a model by a more sophisticated MRMP2, an $S_2/S_1-$CIX is expected to be located at a highly twisted conformation with a quinoid character in the benzene ring. So we conclude that our present model is not so changed by a more sophisticated MRMP2 which is practically prohibited for the moment.

## 4. Concluding Remarks

In the present paper, we proposed a new picture of the photochemical behavior of DMABN in gas phase, nonpolar, and polar solvent by means of CASSCF calculations. The fate of DMABN after the weak transition of $S_0-S_1$ is simple; i.e., the aromatic benzene ring expands with hexagon so that DMABN in $S_1$ directly relaxes into the most stable LE-geometry. On the other hand, the fate after the strong transition of $S_0-S_2$ is more complicated. The key to the elucidation of the mechanism is information on $S_2/S_1-$CIX, which is the relaxation channel from $S_2$ into $S_1$. The $S_2/S_1-$CIX is a crossing region between CT and LE and is characterized by a dimethyl-amino-twisted quinoid structure. The CT-geometry in $S_1$ increases a more quinoid character than $S_2/S_1-$CIX, whereas the dimethyamino part remains perpendicularly twisted. However, the CT-geometry in $S_1$ is not stabilized in gas phase or nonpolar solvent so that DMABN finally relaxes into the most stable LE-geometry through a recrossing at $S_2/S_1-$CIX. On the other hand, the CT-geometry is much stabilized in polar solvent because of large electrostatic interaction, though the process before the relaxation at $S_2/S_1-$CIX is not affected by solvent.

This causes the equilibration between LE- and CT-geometries in $S_1$ takes place and finally relaxes into the CT-geometry. In this equilibration process, both $\tau$-torsional motion and the formation of quinoid structure without aromaticity in the benzene ring are essential factors for the CT state to be stabilized in polar solvent. On the basis of the computational findings of DMABN and its derivatives, we proposed a new and simple guiding principle of the emission properties of DMABN derivatives so as to overcome each defects of conventional PICT and TICT model: *a larger torsional $\tau$ angle and/or a more planar structure at the equilibrium geometry in $S_0$ lead to a better condition for the CT emission*. We give a perspective that our present model will be not so changed even by a more sophisticated MRMP2 method.

**Acknowledgment.** The numerical calculations were partly performed in the Computer Center of Institute for Molecular Science. This work is financially supported by Grant-in-Aid for Scientific Research (C) (No. 15550003) from Japan Society for the Promotion of Science.

## References and Notes

(1) Lippert, E.; Lüder, W.; Moll, F.; Nägele, W.; Boos, H.; Prigge, H.; Seibold-Blankenstein, I. *Angew. Chem.* **1961**, *73*, 695−706.

(2) Rotkiewicz, K.; Grellmann, K. H.; Grabowski, Z. R. *Chem. Phys. Lett.* **1973**, *19*, 315−318.

(3) Köhler, G.; Rechthaler, K.; Rotokiewicz, K.; Rettig, W. *Chem. Phys.* **1996**, *207*, 85−101.

(4) Gude, C. C.; Rettig, W. *J. Phys. Chem. A* **1998**, *102*, 7754−7761.

(5) Rettig, W.; Lutze, S. *Chem. Phys. Lett.* **2001**, *341*, 263−271.

(6) Zachariasse, K. A.; Grobys, M.; Von der Haar, T.; Hebecker, A.; Il'ichev, Y. V.; Morawski, O.; Rückert, I.; Kühnle, W. *J. Photochem. Photobiol. A* **1997**, *105*, 373−383.

(7) Chudoba, C.; Kummrow, A.; Dreyer, J.; Stenger, J.; Nibbering, E. T. J.; Elsaesser, T.; Zachariasse, K. A. *Chem. Phys. Lett.* **1999**, *309*, 357−363.

(8) Zachariasse, K. A. *Chem. Phys. Lett.* **2000**, *320*, 8−13.

(9) Demeter, A.; Druzhinin, S.; George, M.; Haselbach, E.; Roulin, J.-L.; Zachariasse, K. A. *Chem. Phys. Lett.* **2000**, *323*, 351−360.

(10) Daum, R.; Druzhinin, S.; Ernst, D.; Rupp, L.; Schroeder, J.; Zachariasse, K. A. *Chem. Phys. Lett.* **2001**, *341*, 272−278.

(11) Druzhinin, S. I.; Demeter, A.; Galievsky, V. A.; Yoshihara, T.; Zachariasse, K. A. *J. Phys. Chem. A* **2003**, *107*, 8075−8085.

(12) Zachariasse, K. A.; Druzhinin, S. I.; Bosch, W.; Machinek, R. *J. Am. Chem. Soc.* **2004**, *126*, 1705−1715.

(13) Sobolewski, A. L.; Domcke, W. *Chem. Phys. Lett.* **1996**, *250*, 428−436.

(14) Sobolewski, A. L.; Domcke, W. *Chem. Phys. Lett.* **1996**, *259*, 119−127.

(15) Sobolewski, A. L.; Sudholt, W.; Domcke, W. *J. Phys. Chem. A* **1998**, *102*, 2716−2722.

(16) Gorse, A. D.; Pesquer, M. *J. Phys. Chem.* **1995**, *99*, 4039−4049.

(17) Parusel, A. B. J.; Köhler, G.; Grimme, S. *J. Phys. Chem. A* **1998**, *102*, 6297−6306.

(18) Kwok, W. M.; Ma, C.; Phillips, D.; Matousek, P.; Parker, A. W.; Towrie, M. *J. Phys. Chem. A* **2000**, *104*, 4188−4197.

(19) Kwok, W. M.; Ma, C.; Matousek, P.; Parker, C. W.; Phillips, D.; Toner, W. T.; Towrie, M. *Chem. Phys. Lett.* **2000**, *322*, 395−400.

(20) Kobayashi, T.; Futakami, M.; Kajimoto O. *Chem. Phys. Lett.* **1986**, *130*, 63−66.

(21) Kobayashi, T.; Futakami, M.; Kajimoto, O. *Chem. Phys. Lett.* **1987**, *141*, 450−454.

(22) Kajimoto, O.; Yokoyama, H.; Ooshima, Y.; Endo, Y. *Chem. Phys. Lett.* **1991**, *179*, 455−459.

(23) Saigusa, H.; Miyakoshi, N.; Mukai, C.; Fukagawa, T.; Kohtani, S.; Gordon, R. *J. Chem. Phys.* **2003**, *119*, 5414−5422.

(24) Hashimoto, M.; Hamaguchi, H. *J. Phys. Chem.* **1995**, *99*, 7875−7877.

(25) Ma, C.; Kwok, W. M.; Matousek, P.; Parker, A. W.; Phillips, D.; Toner, W. T.; Towrie, M. *J. Phys. Chem. A* **2002**, *106*, 3294−3305.

(26) Okamoto, H.; Inishi, H.; Nakamura, Y.; Kohtani, S.; Nakagaki, R. *J. Phys. Chem. A* **2001**, *105*, 4182−4188.

(27) Fuss, W.; Pushpa, K. K.; Rettig, W.; Schmid, W. E.; Trushin, S. A. *Photchem. Photobiol. Sci.* **2002**, *1*, 255−262.

(28) Kato, S.; Amatatsu, Y. *J. Chem. Phys.* **1990**, *92*, 7241−7257.

(29) Hayashi, S.; Ando, K.; Kato, S. *J. Phys. Chem.* **1995**, *99*, 955−964.

(30) Andrés, S.-L.; Merchán, M.; Roos, B. O.; Lindh, R. *J. Am. Chem. Soc.* **1995**, *117*, 3189−3204.

(31) Mennucci, B.; Toniolo, A.; Tomasi, J. *J. Am. Chem. Soc.* **2000**, *122*, 10621−10630.

(32) Rappoport, D.; Furche, F. *J. Am. Chem. Soc.* **2004**, *126*, 1277−1284.

(33) Amatatsu, Y. *Theor. Chem. Acc.* **2000**, *103*, 445−450.

(34) Amatatsu, Y. *Chem. Phys.* **2001**, *274*, 87−98.

(35) Schmidt, M. W.; Baldridge, K. K.; Boatz, J. A.; Elbert, S. T.; Gordon, M. S.; Jensen, J. H.; Koseki, S.; Matsunaga, N.; Nguyen, K. A.; Su, S. J.; Windus, T. L.; Dupuis, M.; Montgomery, J. A., Jr. *J. Comput. Chem.* **1993**, *14*, 1347.

(36) Frisch, M. J.; Trucks, G. W.; Schlegel, H. B.; Scuseria, G. E.; Robb, M. A.; Cheeseman, J. R.; Montgomery, J. A., Jr.; Vreven, T.; Kudin, K. N.; Burant, J. C.; Millam, J. M.; Iyengar, S. S.; Tomasi, J.; Barone, V.; Mennucci, B.; Cossi, M.; Scalmani, G.; Rega, N.; Petersson, G. A.; Nakatsuji, H.; Hada, M.; Ehara, M.; Toyota, K.; Fukuda, R.; Hasegawa, J.; Ishida, M.; Nakajima, T.; Honda, Y.; Kitao, O.; Nakai, H.; Klene, M.; Li, X.; Knox, J. E.; Hratchian, H. P.; Cross, J. B.; Adamo, C.; Jaramillo, J.; Gomperts, R.; Stratmann, R. E.; Yazyev, O.; Austin, A. J.; Cammi, R.; Pomelli, C.; Ochterski, J. W.; Ayala, P. Y.; Morokuma, K.; Voth, G. A.; Salvador, P.; Dannenberg, J. J.; Zakrzewski, V. G.; Dapprich, S.; Daniels, A. D.; Strain, M. C.; Farkas, O.; Malick, D. K.; Rabuck, A. D.; Raghavachari, K.; Foresman, J. B.; Ortiz, J. V.; Cui, Q.; Baboul, A. G.; Clifford, S.; Cioslowski, J.; Stefanov, B. B.; Liu, G.; Liashenko, A.; Piskorz, P.; Komaromi, I.; Martin, R. L.; Fox, D. J.; Keith, T.; Al-Laham, M. A.; Peng, C. Y.; Nanayakkara, A.; Challacombe, M.; Gill, P. M. W.; Johnson, B.; Chen, W.; Wong, M. W.; Gonzalez, C.; Pople, J. A. *Gaussian 03*, revision B.04; Gaussian, Inc.: Pittsburgh, PA, 2003.

(37) Amatatsu, Y. *J. Compt. Chem.* **2002**, *23*, 928−937.

(38) Amatatsu, Y.; Hasebe, Y. *J. Phys. Chem. A* **2003**, *107*, 11169−11173.

(39) Amatatsu, Y.; Hosokawa, M. *J. Phys. Chem. A* **2004**, *108*, 10238−10244.

(40) Amatatsu, Y. *J. Compt. Chem.* **2002**, *23*, 950−956.

(41) Peter, K.; Vollhardt, C.; Schore, N. E. *Organic Chemistry, Structure and Function*, 3rd ed.; Freeman and Co.: W. H.; New York, 1999; Chapter 3.